



Contents lists available at *Dergipark*

## Journal of Scientific Reports-A

journal homepage: <https://dergipark.org.tr/tr/pub/jsr-a>



**E-ISSN: 2687-6167**

**Number 55, December 2023**

### **RESEARCH ARTICLE**

*Receive Date: 27.07.2023*

*Accepted Date: 16.10.2023*

# Investigation of low-cycle fatigue in adhesively-bonded single-lap joints

Gamze İspirlioğlu-Kara<sup>1,\*</sup>, Adnan Özel<sup>2</sup>

<sup>a\*</sup> *Ataturk University, Faculty of Engineering, Department of Mechanical Engineering, Erzurum and 25240, Turkey, ORCID: 0000-0001-9968-1739*

<sup>b</sup> *Erzincan Binali Yıldırım University, Faculty of Engineering, Department of Mechanical Engineering, Erzincan and 24002, Turkey, ORCID: 0000-0001-8527-3136*

## **Abstract**

The benefits of adhesively bonded joints (ABJs), including their high strength, even stress distribution, and excellent fatigue resistance, make them a viable substitute for traditional mechanical joining techniques like bolts, rivets, welding, and soldering. In industries like aerospace and aviation where weight is a major consideration, these adhesively bonded parts are becoming increasingly significant. ABJs are preferred because they offer highly reliable connections. This work used both experimental and numerical methods to examine the low cycle fatigue of materials built as adhesively-bonded single-lap joints. It is aimed to carry out this study to expand the area of use in areas where weight is critical, such as the aerospace industry. The joints of aluminum and steel specimens were subjected to variable loads with mean failure loads lower than the failure loads obtained experimentally and the number of cycles was determined. As a result, the fatigue life of adhesively bonded single-lap stainless-steel joints was higher than that of aluminum specimens. Additionally, the fatigue life of the steel specimens was found to be greatly extended by putting glue around the joint's endpoints. The fatigue strength increased with increasing adhesive thickness based on test and investigation results. It was also found that pre-filled, ABJs increase the low cycle fatigue strength.

© 2023 DPU All rights reserved.

Keywords: Adhesive; Low-cycle fatigue; Adhesively bonded single-lap joints

\* Corresponding author. Tel.: +0-553-618-29-69.  
E-mail address: [gamze.ispirlioglu@atauni.edu.tr](mailto:gamze.ispirlioglu@atauni.edu.tr)  
<https://orcid.org/0000-0001-9968-1739>

## 1. Introduction

Adhesives are polymeric materials that bind materials to the surface to which they are applied, preventing them from separating. Adhesives are made by combining different materials, and any kind of material can be bonded together with an adhesive. Adhesively bonded joints (ABJs) have been studied for many years. While adhesives were regarded in the early studies as linear elastic materials, the elastoplastic properties of adhesives were also considered in later studies.

ABJs perform poorly against peel stresses despite having good shear characteristics. Eccentric loading in ABJs causes peeling strains in the overlap area, which can lead to damage. Numerous research has attempted to lessen the impacts of peel stresses [1] by creating a variety of strategies, such as altering the geometry of the lap and joint [2], employing scarf joints [3], utilizing composite [4] or curved [5,6] patches in the joints, and creating an adhesive fillet [7].

Sayman et al. conducted an analytical nonlinear elastoplastic stress analysis for an adhesively attached single-acting joint in a different investigation. The impact of the bending moment was disregarded in this investigation. The finite element method (FEM) and the analytical solution were compared, and it was discovered that the outcomes were consistent. According to all of these investigations, the shear and normal stresses have a maximum value at the ends and are constant along the overlap region's center. Because of this, the high strains at the adhesive layer's ends have become increasingly significant in later research, and this phenomenon is frequently referred to as end effects [8].

The failure load of ABJs is significantly influenced by the thickness of the adhesives used in the joining process. As a result, a statistical investigation was conducted to determine how adherend thickness affected the joints' failure load [9–12].

Sawa et al.'s study [13] focused on single-lap joints (SLJs) that integrate adherends from several material kinds. Stress values were reported to be higher in materials having a low modulus of elasticity, and stress accumulation was seen to have occurred close to the interface edges. It was also determined that tension rose when adherend and adhesive thickness dropped.

Gleich et al. [14] varied the adhesive's thickness between 0.1 and 0.5 mm to examine the relationship between the maximum load the joint can support and the thickness. According to the analyses, joint strength rose as adhesive thickness increased. Nonetheless, the study emphasized that stress rises when adhesive thickness falls and vice versa.

The effect of adhesive thickness on adhesion in metal connections was examined by Xu et al. [15] using the "Cohesive Zone Model." The study's findings indicated that as adhesive thickness increases, binding strength falls.

ABJs are subjected to more than just static loads, much like any other conventional joint. Because of the influences of the environment, they are also frequently exposed to dynamic loads. Consequently, it is critical to look at fatigue behaviors. Adhesives enhance the fatigue characteristics of joints by enabling extremely light joints. ABJs are frequently utilized in engineering domains because of the many benefits they provide, the most significant of which is the improvement of fatigue behavior. Several research that looked at the fatigue performance of ABJs could be found in the literature [16–23].

Using DP460 and Al2024-T3 adhesives, Gavgali et al. conducted an experimental and numerical investigation of the static and fatigue strength of SLJs and three-step lap joints. Their investigation revealed that the connection's static and fatigue strengths were raised by the gradual overlap application. The conclusion is that the outcomes of the numerical and experimental studies corroborate one another [18].

Braga et al. compared the fatigue performance of AA2024-T3 Al-Mg-Cu alloy SLJs with ABJs formed with friction stir welding and reported that the latter had superior fatigue strength [24].

In another study, Bayramoğlu et al. investigated the impact of adhesive stresses on material thickness and overlap length using the cohesive zone model and the multilinear isotropic hardening model. The comparison of numerical data with the experimental results revealed that the cohesive zone model was more compatible. The multilinear

isotropic hardening model and the adhesive zone model differ by 7% in terms of the damage load on the adhesive and 32% in terms of displacement, respectively [25].

Hacısalihoglu et al. examined the strength of SLJs made in the bonded material by indenting it in two and three stages with varying thicknesses and lengths. The strength of the joint was enhanced by about 33 to 40 percent by notching and recessing the joints in two or three steps [26].

The tension-tension fatigue behavior of double-lap fiber-reinforced polymer (FRP) joints joined by a ductile adhesive was experimentally studied by Liu et al. [27]. Despite the ductile adhesive's rubbery nature at both ambient and high temperatures, the investigation revealed that the joints exhibited notable sensitivity to loading rate and temperature.

Tan et al. [28] formed thick adhesive shear joints (TASJs) with Sikaflex®-265 polyurethane glue and aluminum and its alloys to investigate the impact of the transition temperature on the adhesive structure's fatigue performance. After noting that the fatigue performance of SLJs progressively declined as the temperature rose, it was determined that temperature did affect the fatigue performance of SLJs. The fatigue performance declines with increasing temperature as it approaches the adhesive's transition temperature.

Experimental research was done on the lives of AA2024-T3 aluminum alloy SLJs made with DP460 adhesive placed at five different adhesive thicknesses under various tensile fatigue loads [29–31]. The investigation showed that as adhesive thickness increased, so did the joints' static tensile strength.

In contrast to previous research published in the literature, this study uses pre-filled steel, aluminum, and steel samples with the same adhesive thickness to investigate low-cycle fatigue in SLJs. To find the load at which steel samples break, tensile tests were performed on them initially with varying adhesive thicknesses. The low-cycle values at which the steel and aluminum samples failed were then ascertained [32] by applying various percentages of the failure load, such as 50% or higher, by the ASTM standard. Ten hertz (Hz) loading rates ( $R = 0$ ) were used for the fatigue tests.

## **2. Experimental Procedure**

### *2.1. Material and Samples*

The study was schemed by a sequential algorithm (Fig. 1) within the framework of the relevant ASTM and ISO standards. First of all, the samples were cut to the determined dimensions, and necessary surface treatments were performed. Then, the bonding of the adherents was made to form SLJs. A low-cycle fatigue test was performed on the joints. The FEM studies carried out in ANSYS were compared with the experimental test results.

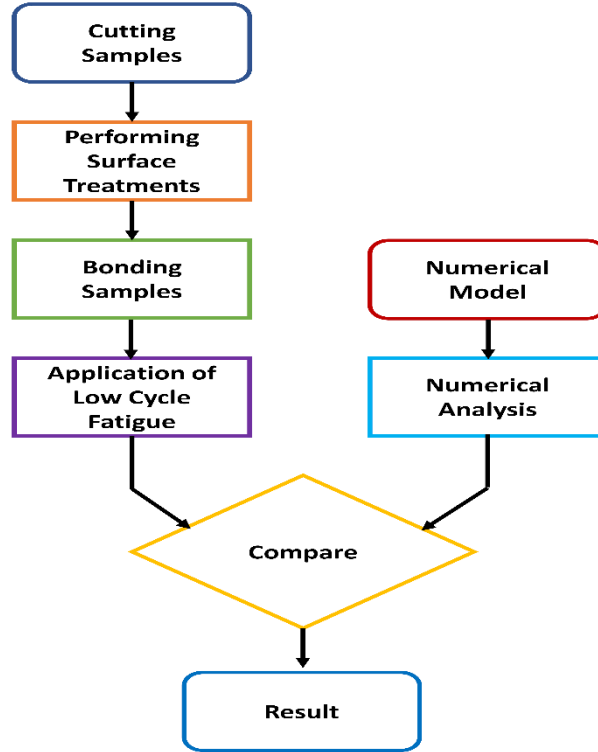


Fig. 1. General schematic of the experimental procedure followed in the study.

In this work, adherents that is, materials to be adhesively bonded were 7075-T7 aluminum alloy and AISI 304 stainless steel. The adhesive utilized in the investigation was 3M brand DP 460, a two-component, liquid epoxy structural adhesive. The joints were kept at 60°C for 120 minutes as per the manufacturer's recommended curing method, which was scrupulously followed. Table 1 displays the samples' and adhesive's mechanical characteristics [6,33].

Table 1. Mechanical properties of samples and adhesive [6,33]

Material	Modulus of Elasticity (MPa)	Poisson Ratio
Aluminum (7075-T7)	73.293	0.33
Steel (AISI 304)	180,000	0.29
Adhesive (DP 460)	2,077	0.38

Samples were cut from aluminum and steel materials in 25x100x5mm dimensions, as shown in Fig. 2(a), and necessary surface treatments were performed to prepare the samples for joining, as seen in Fig. 2(b).

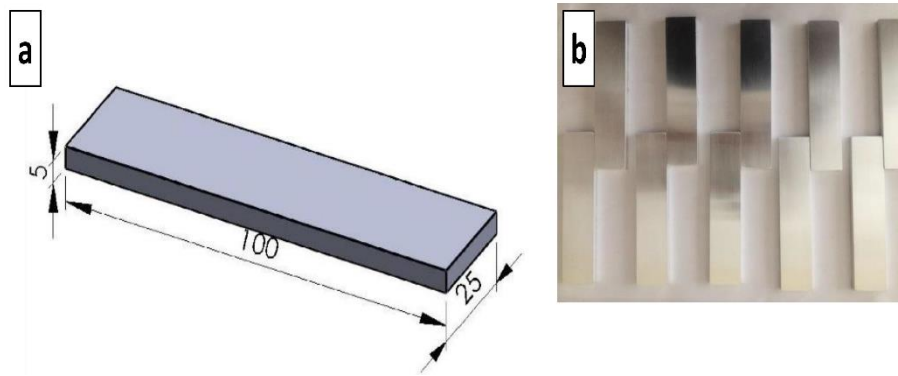


Fig. 2. (a) Sample model; (b) samples after surface preparation processes.

Regarding the strength of the adhesive union, the surfaces that need to be bonded must be properly prepared. The following procedures, in order, were part of the surface preparation process: Sanding papers with a grit of 80 to 1200 was used to deburr and sand the samples. The samples were then cleaned, rinsed, and stored in an acetone bath before being oven-dried. Fig. 2(b) displays the samples that have undergone all surface preparation procedures and are prepared for joining.

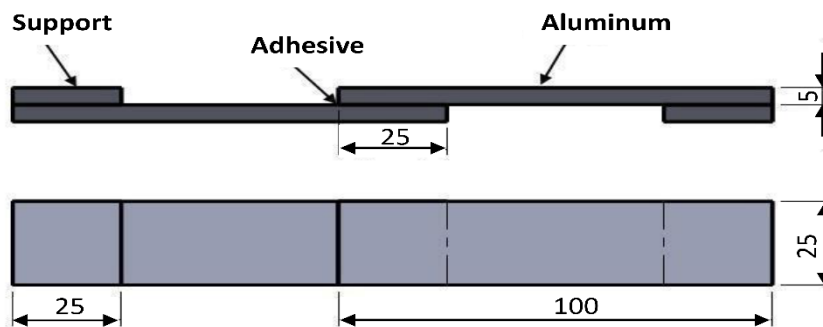


Fig. 3. Dimension and joining details of the adhesively bonded SLJs.

25x100x5mm-sized aluminum and steel samples were adhesively bonded as shown in Fig. 3, with an overlap length of 25mm, and with two pieces of 25x25x5mm-sized supports placed beside the respective ends of each adhered to make sure that the specimens are free from any eccentricity that might occur, as well as eliminating the effects of such eccentricity on the results of the tensile tests.

ISO 15166-1 standard includes issues related to the preparation of bulk samples. This standard specifies the rules to be followed in the preparation of bulk samples from one-component and two-component adhesives. By this standard, bulk samples are prepared from two-component liquid adhesive 3M™ DP 460. For this purpose, a mold consisting of two plates of a certain thickness and a frame placed between them to adjust the thickness of the adhesive layer is used. 3M™ DP 460 liquid adhesive is poured into this mold and pressure is applied using a plate on the mold to bring the adhesive to the desired thickness. After this process, the mold is placed in an oven at 60 °C for 120 minutes, and the necessary curing conditions are applied. Thus, 3M™ DP 460 bulk specimens are produced. To adjust the specimen thickness, a metal U frame with a thickness of 2 mm is prepared and placed on the lower table of the press. Silicone lubricant is sprayed onto the upper and lower tables of the press and the U frame to form

a very thin film. Thus, the adhesion of the bulk adhesive layers on the tables is prevented. The upper table of the press is pressurized until it is fully seated on the U frame and the specimens reach the desired thickness. Thus, the pressure required for the adhesive to cure is applied and the formation of air bubbles is prevented.

Two distinct adhesive thicknesses, 0.1 mm, and 0.2 mm, were tested with the steel samples in the study, while the adhesive thickness of the aluminum and pre-filled steel samples was 0.1 mm. Table 2 presents the classification of the various joints utilized in the trials.

Table 2. Joint types used in the experiment

Material	Type	Remarks
Aluminum	Type I	Aluminum bonded with 0.1mm adhesive thickness
Steel	Type II-a	Steel bonded with 0.1 mm adhesive thickness
Steel	Type II-b	Pre-filled steel bonded with 0.1 mm adhesive thickness
Steel	Type II-c	Steel bonded with 0.2 mm adhesive thickness

To prevent adhesion problems and to enable the connections to form properly, a mold made of AISI 4140 steel was used in the assembly of the joints and during the curing period, as shown in Fig. 4.

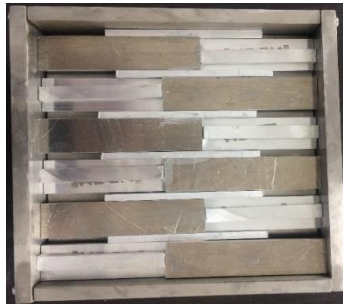


Fig. 4. Assembly of joints in the mold.

The assembly mold consisted of four parts: the lower table, the upper table, the frame, and the supports. The frame of the mold is detachable to allow the samples to be removed from the mold easily. The upper table was designed to ensure proper bonding by applying pressure onto the joints during the curing period of the adhesive. Samples were prevented from bonding to one another using intermediate supports. The upper table of the mold was sealed after the glue was applied and the adherents were joined. The mold was then placed in an oven set to 60°C for two hours to allow the adhesive to dry. The samples were taken out of the oven and let to stand at room temperature for a full day before the studies began, allowing the glue to cure.

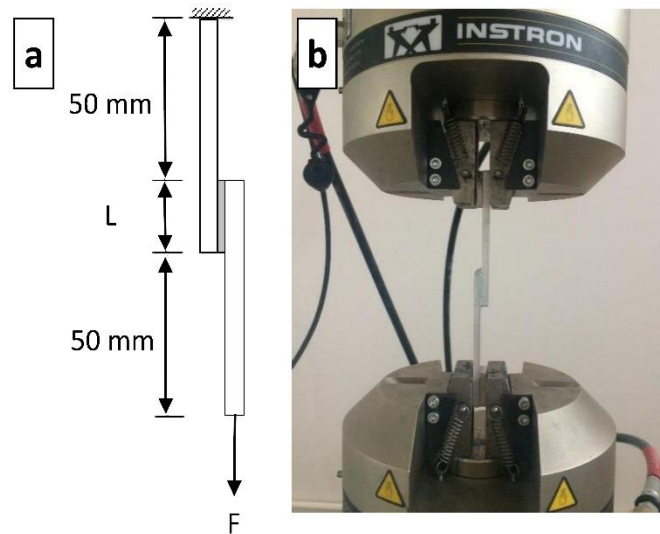


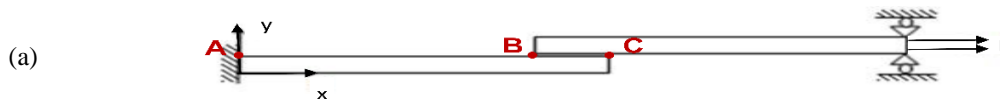
Fig. 5. (a) Boundary conditions and loads used in the tensile test and; (b) tensile loading.

Tensile testing of SLJs specimens was performed on an Instron 8801 fatigue testing system, shown in Fig. 5. All experiments were carried out at room temperature with a jaw speed of 1 mm/min until breakage.

## 2.2. Elastoplastic finite element analysis

Aluminum and steel joints used in the experiments, bonded with 3MTM DP460 adhesive, were modeled in 2-dimensions under tensile load using ANSYS by the Multilinear Isotropic Hardening-von Mises Plasticity (MISO) material model, assuming plane strain conditions. This was done for elastoplastic finite element analysis (FEA). The loads, boundary conditions, and sample dimensions utilized in FEA are also utilized in experimental investigations. The bonding joint was modeled in the three-dimensional analysis utilizing elements (Solid 186), which had 20 nodal points and three degrees of freedom. Bonding divides the overlay region where the operation is conducted into smaller parts, which is crucial for stress distribution.

After the tensile test, the breaking zone was examined, and the maximum load and failure modes that occurred on the samples were recorded. Boundary conditions and mesh details of the FEM applied are shown in Fig. 6.



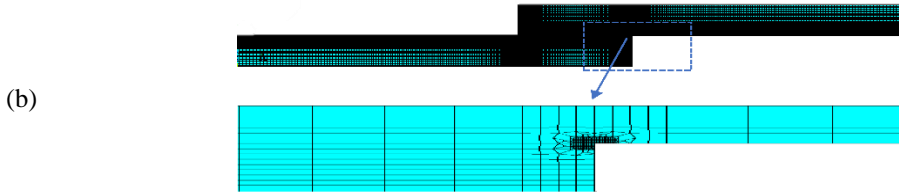


Fig. 6. (a) Boundary conditions and; (b) mesh detail of the FEM applied.

The stresses occurring in the adhesive along the BC line and in the bonded material along the AC line were considered in the analyses. The normal stresses ( $\sigma_x$ ,  $\sigma_z$ ), peel stresses ( $\sigma_y$ ), shear stresses ( $\tau_{xy}$ ), displacements in the direction of the y-axis ( $U_y$ ) and von Mises stresses along the BC line were computed and the effects of these stresses on the joint strength were investigated. Joint types, listed in Table 2, were evaluated comparatively.

### 3. Results and discussion

#### 3.1. Experimental results obtained from samples subjected to tensile load

Adhesively bonded SLJs of aluminum and steel samples were subjected to the tensile test to determine the load under which they broke. Each experiment was repeated 5 times, and the average failure load was calculated and compared for each joint type [30,31]. The accuracy of the average failure load across experiments was 95% (Fig. 7). For Type-II b (0.1 mm adhesive thickness pre-filled steel) joints, very large cycle ratios were obtained for the same loading values. Therefore, they are not shown in Figure 7.

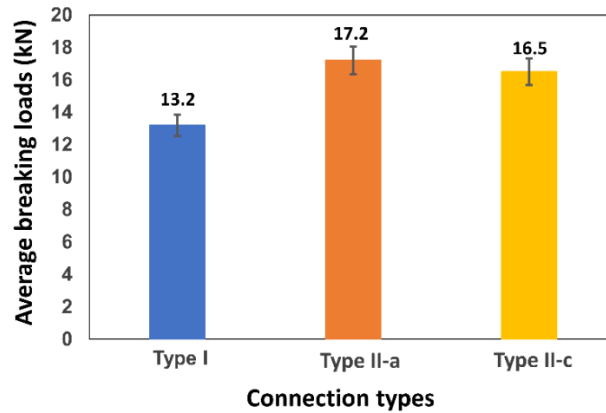


Fig. 7. Average failure loads of the samples.

#### 3.2. Findings of the FEA

The stresses that are most effective on the strength of an adhesively-bonded SLJs are peel stress ( $\sigma_y$ ), normal stresses ( $\sigma_x$ ,  $\sigma_z$ ), and shear stress ( $\tau_{xy}$ ).

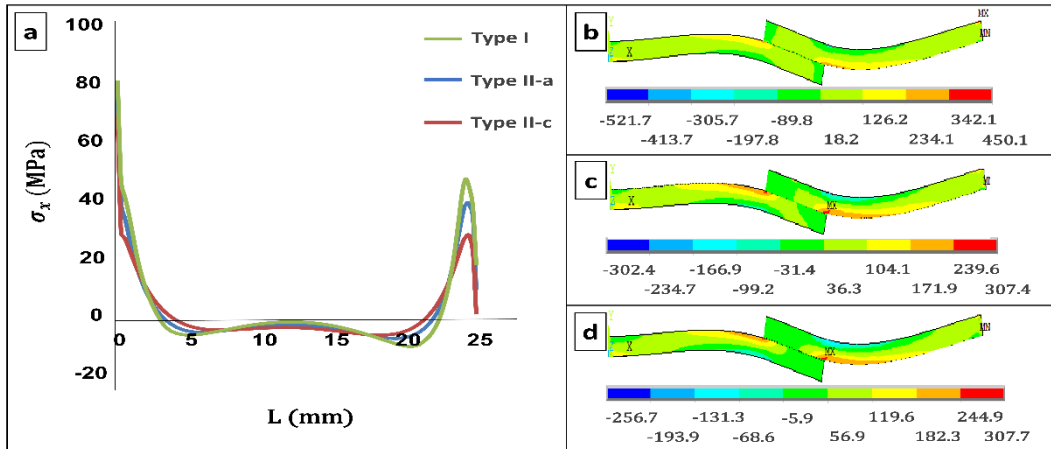


Fig. 8. (a) Distribution of the normal stress in the x-axis ( $\sigma_x$ ) in the adhesive layer along the BC line and deformations and; (b) Type I and; c) Type II-a and; d) Type II-c.

There is a variation in the stresses at the endpoints of the link since one end has fixed support while the other end is mobile. Moment-induced peeling stresses result in a crack at the lap length's edges. Damage is caused by the crack's abrupt development toward the lap zone's core. Peel stresses created a crack at the lap length's edges, around 3 mm from the edges. As the step came to an abrupt stop, the crack grew larger. As can be seen in Figure 8, the peel stresses for the connection are compressive in the center and tensile at the overlap region's margins, approaching zero toward the center [18, 26].

In general, the stress distributions have higher values at the overlap ends, and the stresses converge close to zero from the ends towards the center when the normal stress distributions along the BC line (shown in Fig. 8) are compared in the steel and aluminum samples with varying adhesive thicknesses [31].

It was discovered that the highest stress in aluminum (Type I) at the BC line,  $\sigma_x$ , was 81 MPa. Compared to steel (Type II) stresses, this number is much higher. This explains why aluminum has a lower load capacity. Compared to the steel joint with an adhesive thickness of 0.1 mm (Type II-a), the strains at the ends of the Type II-c steel joint have a lower adhesive thickness. This outcome is in line with research findings in the literature that joints bearing heavier stresses have more adhesive thickness. As anticipated, the joint with a 0.2 mm adhesive thickness in this study was shown to be able to support the highest load [34].

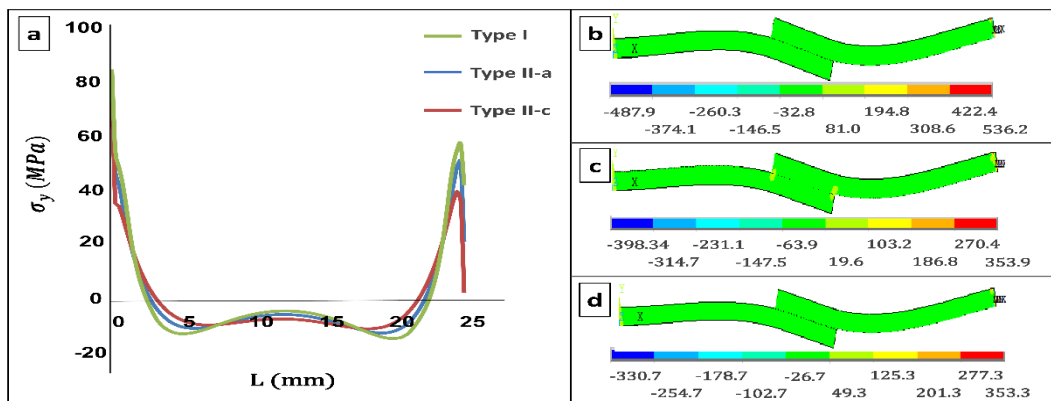


Fig. 9. (a) Distribution of the normal stress in the y-axis ( $\sigma_y$ ) in the adhesive layer along the BC line and deformations and; (b) Type I and; (c) Type II-a and; d) Type II-c.

The end locations of the joint along the BC line are where the peel stresses are at their highest. When it comes to damage occurrence, peel stress ( $\sigma_y$ ) is crucial. The joint's ability to support more weight is increased when this damaging stress is reduced. When comparing the peel stress ( $\sigma_y$ ) distributions shown in Figure 9, the steel sample with a 0.2 mm adhesive thickness (Type II-c) at the BC line's terminal had the lowest stress value. With an increase in adhesive thickness, the peel stress value in the steel sample drops. The joint Type II-c has the maximum load-carrying capability as a result. Conversely, in the Type I aluminum sample, the load-carrying capacity is lower than in other joints because of the peel stress [18,26].

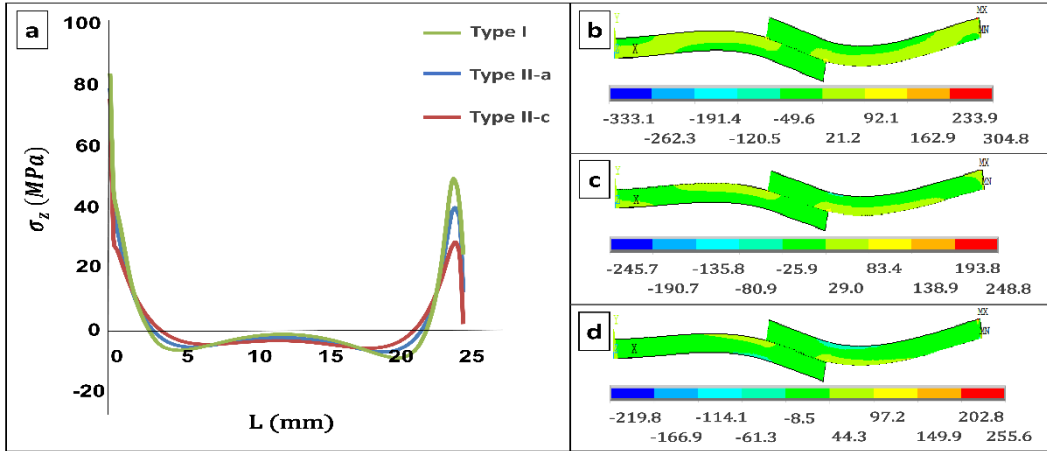


Fig. 10. (a) Distribution of the normal stress in the z-axis ( $\sigma_z$ ) in the adhesive layer along the BC line and deformations and; (b) Type I and; (c) Type II-a and; d) Type II-c.

As seen in Figure 8, the peeling stresses take values close to zero in the center and are compressive towards the center and tensile at the overlap region's boundaries. There are similarities between the stress distribution in the x-axis,  $\sigma_x$ , and the stress distribution in the z-axis,  $\sigma_z$ , as seen in Figure 10.

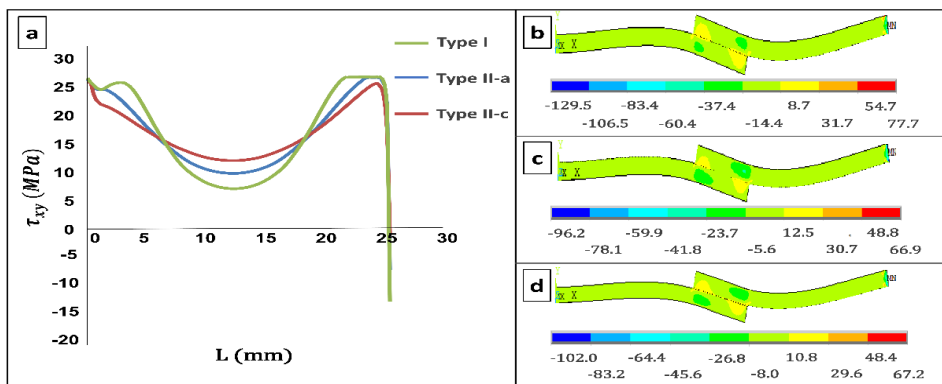


Fig. 11. (a) Distribution of z-axis ( $\tau_{xy}$ ) in the adhesive layer along the BC line and deformations and; (b) Type I and; (c) Type II-a and; d) Type II-c.

Along line BC, shear stresses reach their maximum at the endpoints, whereas in the middle part of the line, this stress value decreases. Examining the shear stress values at point B for aluminum and steel samples, given in Fig. 11, the maximum shear stress value is determined to be around 25 MPa.

The shear stress at point C of the aluminum joint (Type I) takes a negative value of 15 MPa. When the shear stress distribution is examined, it is seen that the load-carrying capacity in the middle part of the adhesive in terms of shear is the lowest in the aluminum sample (Type I) whereas the steel joint with an adhesive thickness of 0.2 mm has the highest. This explains why the load-carrying capacities are different [34].

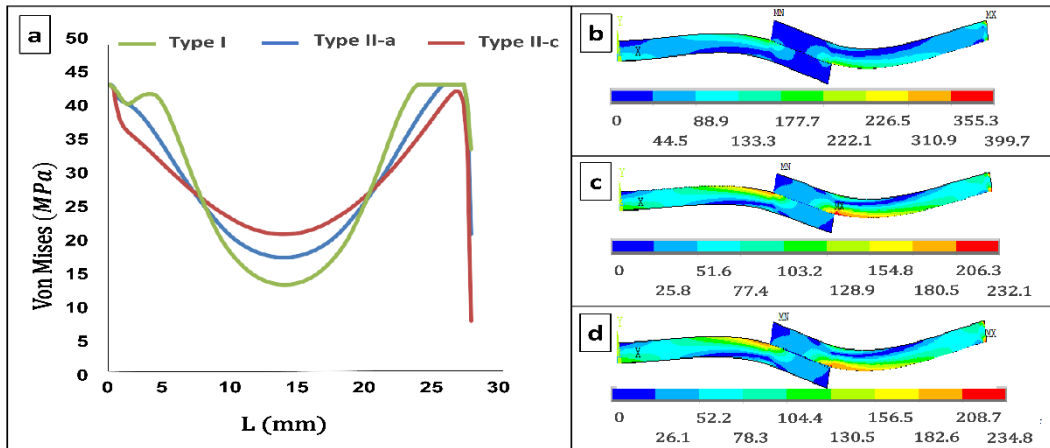


Fig. 12. (a) Distribution von Mises stresses in the adhesive layer along the BC line and deformations and; (b) Type I and; (c) Type II-a and; (d) Type II-c.

Examining Fig. 12, it is seen that the maximum stress value that occurred along the BC line is 45 MPa. Here, as in the shear stress distributions, the lowest load-carrying capacity occurs in the middle parts of the adhesive in the aluminum sample (Type I). The highest load-carrying capacity occurs in the steel sample with an adhesive thickness of 0.2 mm (Type II-c).

Although the stress values at the endpoints of the joints are similar, the difference in the stress distribution in the middle parts affects the load-carrying capacity. Furthermore, no plastic deformation was observed in the adherents of the SLJs subjected to tensile load. The damage initiated at the free ends of the joints and propagated until the joint failed [18,26].

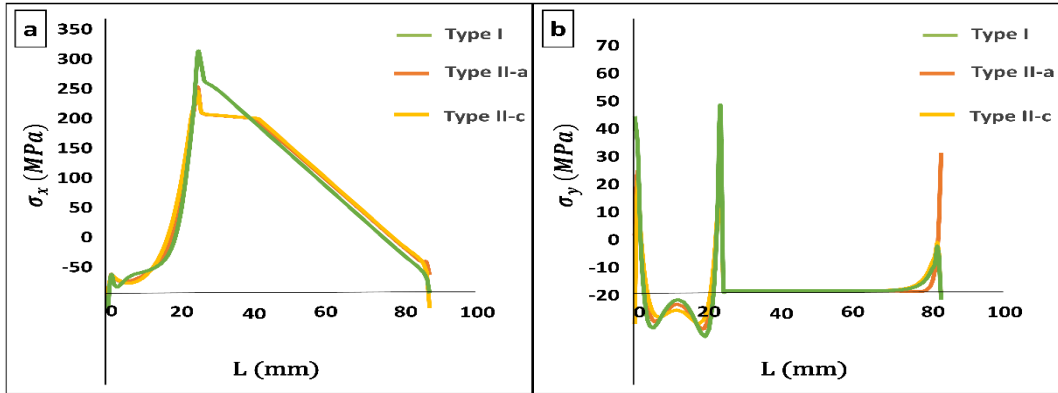


Fig. 13. Distribution of (a) Normal stress ( $\sigma_x$ ) and; (b) Peel stress ( $\sigma_y$ ) along the AC line.

While the distributions of normal stress ( $\sigma_x$ ) and peel stress ( $\sigma_y$ ) along the AC line, given in Fig. 13, generally have low values at the endpoints, the stress values increase from the ends towards the middle. Maximum stresses occur in the transition zone from the joint to the adherend.

While the maximum stress value that occurs in the aluminum sample (Type I) along the AC line is 315 MPa, this value is around 280 MPa in the steel sample (Type II). The distributions of normal stress ( $\sigma_x$ ) in the steel joints with adhesive thicknesses of 0.1 mm (Type II-a and Type II-b) and 0.2 mm (Type II-c) are almost the same. The maximum value of the peel stress ( $\sigma_y$ ) on the AC line that caused damage to the joint was determined to be 55 MPa. Stress accumulations caused by the discontinuities in the adhesive zone can be seen in the graphs. This is particularly evident at the endpoints. No peel stress ( $\sigma_y$ ) occurs in regions other than the bonding zone, which is consistent with the boundary conditions [6,34,35].

No plastic deformation was observed in the materials. The damage initiated at the free ends of the joints and propagated until the joint failed.

### 3.3. Experimental Results Obtained from the Samples Subjected to Fatigue

The average failure loads of aluminum and steel samples were determined through tensile tests performed as per the ASTM 3166-99 standard, which requires the specimen to be subjected to high-cycle fatigue under a load that is equivalent to 50%–45% of its failure load. Since there are no requirements in the relevant standards for low-cycle fatigue testing, the experiments were carried out under 50% or more of the average failure load to examine the low-cycle fatigue behavior of the samples. This test was repeated five times for aluminum, steel, and pre-filled steel samples at each load condition. All tests were for  $R = 0$ , i.e., when the load changes from 0 to 14 kN,  $F_{\max} = 14$  kN, and  $F_{\min} = 0$ , both the amplitude of the force and the average force are equal to 7 kN. The average number of cycles for Type I, Type II-a, Type II-b, and Type II-c is presented in Fig. 14 [31,35].

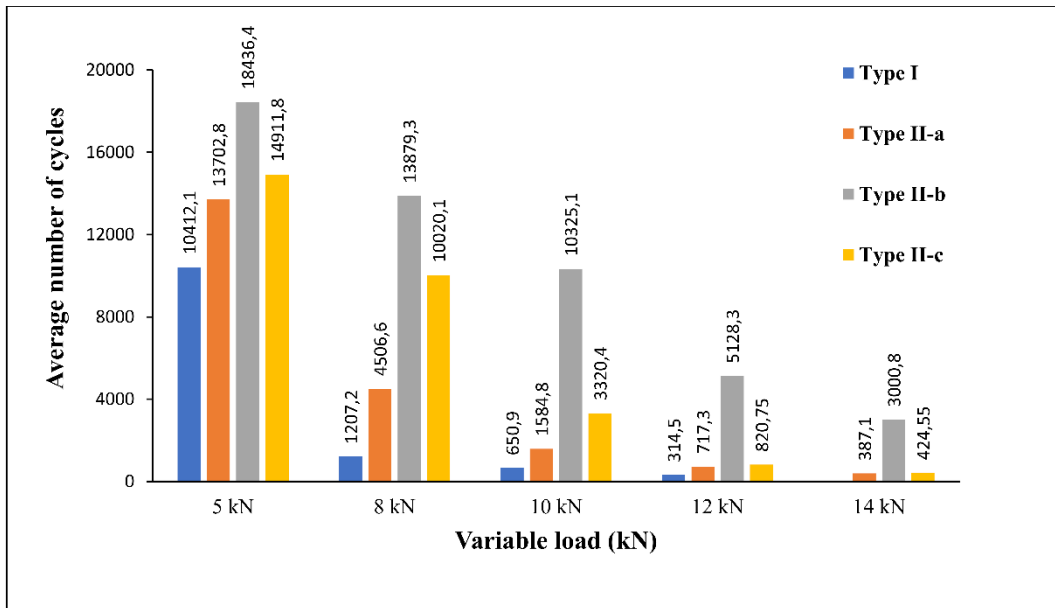


Fig. 14. Average number of cycles for Type I, Type II-a, Type II-b, and Type II-c.

In the Type-I joint, a 12 kN load corresponds to 90% of the average failure load, whereas 10 kN corresponds to 75%, 8 kN to 60%, and 5 kN to 38%. When the load was decreased from 12 kN to 10 kN, the increase in fatigue life was approximately two-folds as great, although the percentage of the change in load is approximately 15%. Likewise, when the load was decreased from 10 kN to 8 kN, where the change in the load was 20%, the increase in the number of cycles was slightly below two-folds. With the load decreased to 5 kN, which corresponds to 38% of the average failure load, the fatigue life moved into the high-cycle region.

In the Type-II joint, a 14 kN load corresponds to 81% of the average failure loads, whereas 12 kN corresponds to 75%, 10 kN to 58%, and 8 kN to 46.5%. In the Type-II-b joint, very large cycle numbers were obtained for the same load values compared to the Type-II-a joint. For example, for a 14 kN load, pre-filling with adhesive increased the number of cycles by 7.75-folds, even though all other properties of the samples were the same.

In the Type-II c joint, a 14 kN load corresponds to 85% of the average failure load, whereas 12 kN corresponds to 75%, 10 kN to 60%, and 8 kN to 49%. When the load was decreased from 14 kN to 12 kN, where the percentage of the change in load is 14%, the increase in fatigue life was approximately 1.85-folds. Likewise, when the load was decreased from 12 kN to 10 kN, the change in the load was approximately 16%, and the increase in the number of cycles was more than two-fold as great. When the load was decreased from 10 kN to 8 kN, which means the decrease in the load was 20%, the increase in the number of cycles was 2.85-folds. With the 5 kN load, on the other hand, fatigue life moved into the high-cycle region [34,35].

Even though the increase in the failure load obtained by increasing the adhesive thickness from 0.1 mm to 0.2 mm was just 4%, the increase in the number of cycles, in return, came about to be much greater and increased disproportionately as the load value decreased. For example, while the number of cycles under an 8 kN load was 4506.6 in Type II-a, it exceeded 10,000 in Type II-c under the same load.

#### 4. Conclusions

Experimental and numerical research was done on the mechanical characteristics of SLJ configurations made of steel and aluminum samples that were subjected to tensile loads. The low-cycle fatigue testing of SLJs made of steel and aluminum, with varying adhesive thicknesses, produced the following findings:

The steel samples, which can carry a higher static load, can also withstand a higher number of cycles than the aluminum sample.

It was found that pre-filling, adhesive joints increased the low cycle fatigue strength.

The adhesive thickness was shown to affect the bonding strength in ABJs. When SLJs of steel materials with different adhesive thicknesses were compared, the fatigue strength was found to have increased with the adhesive thickness.

Furthermore, the surfaces of the failure zones in the joints were examined, and the failures were identified to be, generally, of cohesive and special cohesive failure modes.

#### Acknowledgment

This research has been supported by Erzincan Binali Yıldırım University and Atatürk University. The authors would like to express their gratitude to the respective institutions for funding this project.

#### References

- [1] da Silva LFM, Adams RD. Techniques to reduce the peel stresses in adhesive joints with composites. *Int J Adhes Adhes* 2007;27:227–35. <https://doi.org/10.1016/J.IJADHADH.2006.04.001>.
- [2] Gültekin K, Akpınar S, Özel A. The effect of the adherend width on the strength of adhesively bonded single-lap joint: Experimental and numerical analysis. *Compos Part B Eng* 2014;60:736–45. <https://doi.org/10.1016/J.COMPOSITESB.2014.01.022>.
- [3] Adin H. The effect of angle on the strain of scarf lap joints subjected to tensile loads. *Appl Math Model* 2012;36:2858–67. <https://doi.org/10.1016/J.APM.2011.09.079>.
- [4] Akpınar S. The effect of composite patches on the failure of adhesively-bonded joints under bending moment. *Appl Compos Mater* 2013;20:1289–304. <https://doi.org/10.1007/S10443-013-9335-6/FIGURES/16>.
- [5] Zhao X, Adams RD, Da Silva LFM. Single lap joints with rounded adherend corners: Experimental results and strength prediction. *J Adhes Sci Technol* 2011;25:837–56. <https://doi.org/10.1163/016942410X520880>.
- [6] Akpınar S. Effects of Different Curvature Patches on the Strength of Double-Strap Adhesive Joints. <Http://DxDoiOrg/101080/002184642013769098> 2013;89:937–47. <https://doi.org/10.1080/00218464.2013.769098>.
- [7] Doru MO, Özel A, Akpınar S, Aydın MD. Effect of the Spew Fillet on Adhesively Bonded Single-Lap Joint Subjected to Tensile Loading: Experimental and 3-D Non-Linear Stress Analysis. <Http://DxDoiOrg/101080/002184642013777900> 2013;90:195–209. <https://doi.org/10.1080/00218464.2013.777900>.
- [8] Sayman O, Ozen M, Korkmaz B. Elasto-plastic stress distributions in adhesively bonded double lap joints. *Mater Des* 2013;45:31–5.
- [9] El Zaroug M, Kadioglu F, Demiral M, Saad D. Experimental and numerical investigation into strength of bolted, bonded and hybrid single lap joints: Effects of adherend material type and thickness. *Int J Adhes Adhes* 2018;87:130–41. <https://doi.org/10.1016/J.IJADHADH.2018.10.006>.
- [10] Khoramshad H, Akhavan-Safar A, Ayatollahi MR, Da Silva LFM. Predicting static strength in adhesively bonded single lap joints using a critical distance based method: Substrate thickness and overlap length effects. <Http://DxDoiOrg/101177/1464420716666427> 2016;231:237–46. <https://doi.org/10.1177/1464420716666427>.
- [11] Karachalios EF, Adams RD, Da Silva LFM. The behaviour of single lap joints under bending loading. <Http://DxDoiOrg/101080/016942432012761926> 2013;27:1811–27. <https://doi.org/10.1080/01694243.2012.761926>.
- [12] Katnam KB, Crocombe AD, Khoramshad H, Ashcroft IA. Load Ratio Effect on the Fatigue Behaviour of Adhesively Bonded Joints: An Enhanced Damage Model. <Http://DxDoiOrg/101080/00218460903462632> 2010;86:257–72. <https://doi.org/10.1080/00218460903462632>.
- [13] Sawa T, Liu J, Nakano K, Tanaka J. A two-dimensional stress analysis of single-lap adhesive joints of dissimilar adherends subjected to tensile loads. <Http://DxDoiOrg/101163/156856100742104> 2012;14:43–66. <https://doi.org/10.1163/156856100742104>.
- [14] Gleich DM, Van Tooren MJL, Beukers A. Analysis and evaluation of bondline thickness effects on failure load in adhesively bonded structures. <Http://DxDoiOrg/101163/156856101317035503> 2012;15:1091–101. <https://doi.org/10.1163/156856101317035503>.
- [15] Xu W, Wei Y. Influence of adhesive thickness on local interface fracture and overall strength of metallic adhesive bonding structures. *Int J Adhes Adhes* 2013;40:158–67. <https://doi.org/10.1016/J.IJADHADH.2012.07.012>.
- [14] Pascoe JA, Zavatta N, Troiani E, Alderliesten RC. The effect of bond-line thickness on fatigue crack growth rate in adhesively bonded joints. *Eng Fract Mech* 2020;229:106959. <https://doi.org/10.1016/J.ENGFRACMECH.2020.106959>.

- [17] Sahin R, Akpınar S. The effects of adherend thickness on the fatigue strength of adhesively bonded single-lap joints. *Int J Adhes Adhes* 2021;107. <https://doi.org/10.1016/J.IJADHADH.2021.102845>.
- [18] Gavkali E, Sahin R, Akpınar S. An investigation of the fatigue performance of adhesively bonded step-lap joints: An experimental and numerical analysis. *Int J Adhes Adhes* 2021;104:102736. <https://doi.org/10.1016/J.IJADHADH.2020.102736>.
- [19] Mariam M, Afendi M, Abdul Majid MS, Ridzuan MJM, Gibson AG. Tensile and fatigue properties of single lap joints of aluminium alloy/glass fibre reinforced composites fabricated with different joining methods. *Compos Struct* 2018;200:647–58. <https://doi.org/10.1016/J.COMPSTRUCT.2018.06.003>.
- [20] Liu Y, Lemanski S, Zhang X, Ayre D, Nezhad HY. A finite element study of fatigue crack propagation in single lap bonded joint with process-induced disbond. *Int J Adhes Adhes* 2018;87:164–72. <https://doi.org/10.1016/J.IJADHADH.2018.10.005>.
- [21] Saraç İ, Adin H, Temiz Ş. Experimental determination of the static and fatigue strength of the adhesive joints bonded by epoxy adhesive including different particles. *Compos Part B Eng* 2018;155:92–103. <https://doi.org/10.1016/J.COMPOSITESB.2018.08.006>.
- [22] Takiguchi M, Yoshida F. Effects of Loading Speed and Shear Prestrain on Adhesive Fatigue Strength in Single-Lap Joint. *Key Eng Mater* 2007;340–341:1479–84. <https://doi.org/10.4028/WWW.SCIENTIFIC.NET/KEM.340-341.1479>.
- [23] Yang QD, Shim DJ, Spearing SM. A cohesive zone model for low cycle fatigue life prediction of solder joints. *Microelectron Eng* 2004;75:85–95. <https://doi.org/10.1016/J.MEE.2003.11.009>.
- [24] Braga DFO, Maciel R, Bergmann L, da Silva LFM, Infante V, dos Santos JF, et al. Fatigue performance of hybrid overlap friction stir welding and adhesive bonding of an Al- Mg- Cu alloy. *Fatigue Fract Eng Mater Struct* 2019;42:1262–70.
- [25] Bayramoğlu S, Akpınar S, Çalık A. Numerical analysis of elasto-plastic adhesively single step lap joints with cohesive zone models and its experimental verification. *J Mech Sci Technol* 2021;35:641–9.
- [26] Hacısalihoğlu İ, Akpınar S. The effect of stepped notches and recesses on joint strength in adhesive bonded joints: Experimental and numerical analysis. *Theor Appl Fract Mech* 2022;119:103364.
- [27] Liu L, Wang X, Wu Z, Keller T. Tension-tension fatigue behavior of ductile adhesively-bonded FRP joints. *Compos Struct* 2021;268:113925. <https://doi.org/10.1016/J.COMPSTRUCT.2021.113925>.
- [28] Tan W, Na J, Wang G, Xu Q, Shen H, Mu W. The effects of service temperature on the fatigue behavior of a polyurethane adhesive joint. *Int J Adhes Adhes* 2021;107:102819. <https://doi.org/10.1016/J.IJADHADH.2021.102819>.
- [29] Sahin R, Akpınar S. The effects of adherend thickness on the fatigue strength of adhesively bonded single-lap joints. *Int J Adhes Adhes* 2021;107:102845.
- [30] Akpınar S, Sahin R. The fracture load analysis of different material thickness in adhesively bonded joints subjected to fully reversed bending fatigue load. *Theor Appl Fract Mech* 2021;114:102984. <https://doi.org/10.1016/J.TAFMEC.2021.102984>.
- [31] Sahin R, Akpınar S. The effects of adherend thickness on the fatigue strength of adhesively bonded single-lap joints. *Int J Adhes Adhes* 2021;107:102845. <https://doi.org/10.1016/J.IJADHADH.2021.102845>.
- [32] ASTM. D3166–99. Standard Test Method for Fatigue Properties of Adhesives in Shear by Tension Loading (2012) Google Scholar n.d.
- [33] Demir K, Bayramoğlu S, Akpınar S. The fracture load analysis of different support patches in adhesively bonded single-lap joints. *Theor Appl Fract Mech* 2020;108:102653. <https://doi.org/10.1016/J.TAFMEC.2020.102653>.
- [34] Gültekin K, Akpınar S, Özel A. The effect of moment and flexural rigidity of adherend on the strength of adhesively bonded single lap joints. *J Adhes* 2015;91:637–50.
- [35] Akpınar S. Effects of Different Curvature Patches on the Strength of Double-Strap Adhesive Joints. <http://DxDoiOrg/101080/002184642013769098> 2013;89:937–47. <https://doi.org/10.1080/00218464.2013.769098>.